The Effects of Humidity on Dielectric Permittivity of Surface Modified TiO_2 and MgO Based Polypropylene Nanocomposites

Phichet Ketsamee, Thomas Andritsch and Alun Vaughan

***Abstract*—This work reports on the effects of titanium dioxide (TiO_2) and magnesium oxide (MgO) nanofillers modified with polar silane coupling agents (SCA) on the dielectric response of polypropylene (PP) nanocomposites, in the presence of water molecules. Thermogravimetric analysis demonstrates that the surface structure of the SCA layer between TiO_2 and MgO is significantly different, since the SCA graft density of MgO is 10 times higher than for TiO_2. Surface modified nanofillers tend to agglomerate and that the distribution is determined by the polarity of the surface functional groups. Agglomerations in methacrylate systems are similar in size to those found in untreated samples (3–5 µm), while those with amino functional groups are reduced to 1–2 µm. Nanoparticles also act as nucleating agents, which increases the crystallization temperature by 7–8 °C compared to neat PP. The measured increase in relative permittivity in the composites is attributed to absorbed water. Surface modification significantly reduces this increase, especially in MgO samples. Relaxation peak frequencies vary, depending on the water bonding states, due to differences in polarities of the respective surface functional groups. Two overlapping dielectric mechanisms of dipolar and interfacial relaxation can be detected, especially at low frequencies (20 µHz) in TiO_2 samples. Ethoxy–modified samples containing amino functional groups have the lowest dielectric permittivity under humid conditions.**

***Index Terms*—dielectric permittivity, humidity, polar silane coupling agent, polypropylene, surface modified nanofiller**

I. Introduction

POLPROPYLENE (PP) nanocomposites have been proposed as a potential insulating material for next-generation high voltage cables. It is established that large interface areas are formed between the polymer matrix and nanofiller, which has been linked with improved bulk dielectric properties. For example, Cao *et al*. produced PP containing 1% by weight of magnesium oxide (MgO), leading to enhanced DC breakdown strength (BDS) [1]. Yu *et al*. demonstrated a 4.7% increase in AC breakdown strength in PP with 3 wt.% MgO [2].

Nanoparticles are, in principle, incompatible with nonpolar PP, making a uniform nanoparticle dispersion difficult to achieve in practice. Agglomerations occur easily during processing, which, in turn, affects the dispersion state and interaction with the polymer matrix. This potentially degrades key dielectric properties, while other properties, such as thermal conductivity for example, can benefit from such agglomerates.

Typically, a surface modified nanofiller is required in order to improve particle dispersion and its interaction with the polymer matrix. For example, Abdel-Gawad *et al*. [3] compared two silane coupling agents (SCA) on titanium dioxide (TiO_2) in polyvinyl chloride (PVC). The results showed that PVC coated with vinyl SCA has a higher BDS compared to amino–coated SCA. The authors correlate the improved dispersion of nanoparticles with the enhanced dielectric properties. Conversely, Wang *et al*. demonstrated that aluminum nitride (AlN) modified with polar methacrylate SCA in a PP matrix led to a poor AlN dispersion, in comparison to nonpolar alkane SCA, trimethoxy(octyl)silane (C8–M) and triethoxy(octyl) silane (C8–E) [4]. However, polar methacrylate SCA–treated samples had higher AC BDS. It seems that nanoparticle dispersion cannot be directly correlated with BDS, other parameters such as the type of surface functionalization are also crucial for tailoring dielectric properties.

Although nanoparticles have been shown to improve the dielectric properties of PP systems, selecting the right nanoparticles for PP is particularly challenging, in contrast to popular polyethylene (PE)–based nanocomposites. Different nanoparticles were previously investigated: Zhou *et al*. investigated the effects of MgO, TiO_2, zinc oxide (ZnO), and aluminum oxide (Al_2O_3) on the dielectric properties of PP [5]. They observed that MgO and ZnO resulted in lower dielectric loss than in unfilled PP, while TiO_2 increased the loss, and Al_2O_3 had little measurable effect. Despite the increased dielectric loss, TiO_2 nanocomposites had the highest DC BDS and significant space charge suppression. It is apparent that MgO and TiO_2 are better options than ZnO and Al_2O_3 for enhancing dielectric properties of PP. Table I lists the dielectric performance with different SCA of TiO_2 and MgO in PP nanocomposites.

The measured dielectric properties of nanocomposites are sensitive to absorbed water molecules. Lau *et al*. reported that exposure of PE–based nanocomposites containing 10 wt.% of

This paragraph of the first footnote will contain the date on which you submitted your paper for review, which is populated by IEEE. *(Corresponding author: Phichet Ketsamee).*

Phichet Ketsamee, Thomas Andritsch and Alun Vaughan are with The Tony Davies High Voltage Laboratory, School of Electronics and Computer Science, University of Southampton, Southampton, SO17 1BJ, United Kingdom, (e-mail: pk1r18@soton.ac.uk).

silica (SiO_2) to water led to a 2% increase in mass, compared to unfilled PE, increasing the measured dielectric permittivity in the nanocomposite [6]. This water absorption was reduced to less than 1%, and thus the dielectric permittivity reduced, after surface modification with trimethoxy(propyl)silane, replacing hydroxyl surface groups on the SiO_2 with propyl groups.

In this work, three polar SCA with different organofunctional and hydrolysable groups were used to modify the surface of TiO_2 and MgO nanofillers, which are less prone to oxidation than e.g., the aforementioned AlN investigated in earlier work. This allows for clear distinction of the effects of nanoparticles and the type of SCA, and thus the humidity absorption, on the dielectric properties of PP nanocomposites. Thermal degradation behavior of treated nanoparticles from thermogravimetric analysis (TGA) measurement is used to evaluate the surface functionalization. Scanning electron microscopy (SEM) is implemented to examine nanofiller distribution and dispersion in the composites. Finally, melting and crystallization temperatures are investigated using differential scanning calorimetry (DSC).

II. Materials And Sample Preparations

A. Materials

TiO_2 and MgO nanofillers with the same aspect ratio (spherical) and mean particle size of 10–30 nm were purchased from SkySpring Nanomaterial, Inc. The polar SCA used were: 3–trimethoxysilyl propyl methacrylate (MM), from Sigma Aldrich; 3–aminopropyltrimethoxy silane (MA) and 3–aminopropyltriethoxy silane (EA) from Aladdin industrial Inc. The polymer was isotactic PP, obtained from Sigma Aldrich.

B. Surface Modification of Nanoparticles and Nanocomposite Preparations

An anhydrous technique was used for filler surface treatment, to minimize SCA condensation. The nanoparticle powder was first mixed with toluene and sonicated for 1 h, before the SCA was added to the mixture and stirred for 4 h with a magnetic stirrer. Surface modified nanoparticles were then obtained by centrifugation and washed three times with toluene to remove any excess SCA. After drying for 24 h in a fume cupboard, the resulting material was placed in a vacuum oven for a day to remove any residual solvent.

Nanocomposites were prepared using a solution blending method in which PP pellets were dissolved in hot xylene, while the required mass of nanoparticles was, in parallel, dispersed in xylene and sonicated for 30 min. The particle/xylene mixture was added to the boiling PP/xylene solution and stirred for 1 min. The polymer/nanofiller system was recovered by precipitation in methanol, before being dried in a fume cupboard for 24 h at first, and then stored for 3 d in a vacuum oven. A hydraulic press was used to melt the resulting solid and press it into a thin film, which was quenched in distilled water at room temperature. All samples were stored under vacuum to avoid moisture absorption prior to any measurements. Samples are denoted PP/nanofiller/SCA/filler content/environmental condition, e.g., PP/MgO/MA/5/D. This indicates that PP was mixed with 5 wt.% MgO coated with 3–aminopropyl trimethoxy and was dry (D); H denotes exposure to humidity.

III. Characterization

A. Characterization Techniques

The degradation behavior of treated nanoparticles was measured using a Pyris 1 TGA thermogravimetric analyzer: 3 mg of nanoparticles were placed in a platinum pan and heated from 50 °C to 900 °C at a rate of 10 °C/min in a nitrogen atmosphere.

Scanning electron micrographs were obtained using a Zeiss EVO50XVP using a 20 kV accelerating voltage. Permanganic etching for 10 h using a 1% solution of potassium permanganate in an acid mix composed of 5 parts concentrated sulphuric acid, 2 parts orthophosphoric acid and 1 parts water was used to prepare SEM samples. They were then placed on sample holders and coated with a thin gold layer using an Emitech K550X sputter coater at 25 mA current for 3 min.

A Mettler Toledo DSC–820 differential scanning calorimeter was used to investigate the melting and crystallization behavior of the materials. Approximately 5 mg of a sample was sealed in an aluminum and heated from 20 °C to 200 °C, held at 200 °C for 5 min and cooled from 200 °C to 20 °C. The heating and cooling steps were both conduced at 10 °C/min. All measurements were carried out in a nitrogen atmosphere.

Dielectric data according to ASTM D150–11 [7] were obtained using an Omicron SPECTANO 100 Dielectric Material Analyzer together with a Solartron 1296 2A sample holder. An AC output voltage of 200 V was applied. The polarization depolarization current (PDC) mode was used at frequencies less than 100 mHz, since this offers faster measurements than frequency domain spectroscopy (FDS). The frequency range was 10 mHz to 5 kHz at 8 points per decade in FDS mode and 10 point per decade in PDC mode.

B. Water Absorption

Samples containing either 5 wt.% of TiO_2 or 5 wt.% of MgO were chosen to investigate the effects of water absorption. Gold–coated samples with dimension 40x40 mm^2 and a thickness of 200±10 µm were prepared. Dried materials were immersed in 1 cm of de–ionized water in a Petri dish and sample weight was recorded periodically. The samples were extracted from the water, surface water was removed, and the materials weighed on a microbalance with a precision of 0.0001 g. This method was repeated until a change in mass of <0.1% was achieved. The water uptake, $\%W_H$ represented by the percentage change in sample mass, was calculated by (1).

$$\%W_H = \left|\frac{M_H - M_D}{M_D}\right| \times 100\% \quad (1)$$

where M_D and M_H are the weight of samples under dry and humid conditions, respectively.

TABLE I
DIELECTRIC PERFORMANCE WITH DIFFERENT SCA OF TiO_2 AND MgO IN PP NANOCOMPOSITES.

PP Nanocomposite	Silane Coupling Agent	Filler Content (wt.%)	Mean Size (nm)	Suitable Content (wt.%)	Key Finding	Ref.
PP/MgO	MA	0.5, 1, 3, 6	NA	1	○ DC breakdown strength increased by 30.8% at 1 wt.% MgO compared to unfilled PP. ○ Charge accumulation and field distortion were reduced compared to neat PP up to 1 wt.% MgO.	[1]
PP/MgO	MM	1, 3, 5	50	3	○ DC breakdown strength enhanced 29% at 3 wt.% MgO than neat PP. ○ Space charge was suppressed with nano–MgO content up to 3 wt.%.	[5]
PP/TiO_2	MM	1, 3, 5	50	1	○ DC breakdown strength increased 43% at 1 wt.% TiO_2 compared to neat PP. ○ Charge accumulation was suppressed with nano–TiO_2 content up to 1 wt.%.	[5]
PP/MgO	MM	1, 3, 5	50	3	○ Compared to neat PP, DC breakdown strength rose by 30% at 3 wt.% MgO in 30–90 °C range. ○ Deep traps led to suppressed charge accumulation under high temperatures and electric fields.	[8]
PP/TiO_2	EA	0.5, 1, 3, 5	40	0.5	○ Charge accumulation was suppressed due to the introduction of shallow traps in the materials. ○ Higher charge mobility from the shallow traps increase led to an increase in conduction current.	[9]
PP/TiO_2	C8-M	0.5, 1, 1.5, 2	NA	1	○ DC breakdown strength increased by 20.8% when the nano–TiO_2 was up to 1 wt.%. ○ Charge penetration can be observed in materials only 2 wt.% nano–TiO_2.	[10]

IV. RESULTS AND DISCUSSION

A. Thermogravimetric Analysis

Fig. 1 shows the TGA–measured weight loss of surface modified TiO_2 and MgO nanoparticles. For both the TiO_2 and MgO nanoparticles, the largest mass loss is recorded for MM functionalized particles, followed by MA and EA. When comparing TiO_2 and MgO nanoparticles functionalized with the same SCA, in all cases a significantly larger mass loss in the case of MgO can be observed.

For any given nanoparticle/SCA system with known surface area, if the mass loss associated with degradation of the organic component of the system is known, then the surface density of SCA can be evaluated. For TiO_2, if the effective particle diameter is 20 nm, based on supplier data, then this leads to an SCA graft density that falls in the range 3 to 4 nm^{-2} for all three SCA systems. The surface chemistry of metal oxide nanoparticles such as TiO_2 is dominated by hydroxyl groups –OH [11] [12]. Albeit, the presence of other oxygen–containing moieties (e.g., –C=O, –O– and –COOH) has also been reported [13]. The precise surface chemistry will also depend on the material supplier being used and how it was synthesised, such as demonstrated for different TiO_2 surfaces in literature [12]. While quantitative data pertaining to the precise surface chemistry of TiO_2 is scarce, other nanoparticle systems have been studied extensively. For example in the case of silica, a typical value for the hydroxyl group surface density is ~5 nm^{-2} [14]. An SCA density value of 3–4 nm^{-2} is, therefore, not unreasonable, given that grafting involves the reaction of silanol groups from the SCA with surface hydroxyls.

Repeating the calculation for MgO for the same effective particle diameter, gives a value for the SCA graft density that is close to 30 nm^{-2} for all three systems. This calculated value is significantly higher and most likely an over–estimation of the real value. However, based on the observed test results it would appear that the graft density would be significantly higher for MgO than for TiO_2. To address the concern of overestimating the graft density, a sensitivity analysis was undertaken which demonstrates that a comparable SCA graft density in TiO_2 could only be achieved if the effective MgO nanoparticle diameter would be of the order of 2 nm, which is unrealistic. As such it can be concluded that the surface structure of the SCA layer differs significantly between TiO_2 and MgO.

B. Scanning Electron Microscopy

Fig. 2 shows representative SEM micrographs of etched surfaces of PP nanocomposites. Both systems with untreated particles contain aggregations 3–5 μm in size. Although the dispersion in the MM systems appears better than in the untreated system, in neither case was the distribution of particles uniform within the matrix. Agglomerations of a similar size to untreated samples could be observed. This is consistent with the results of [15], which showed that coating

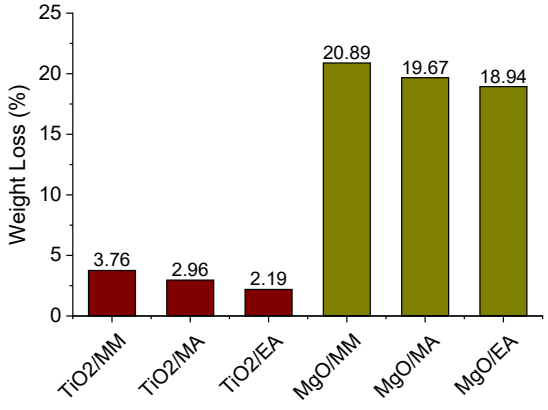

Fig. 1. Weight loss of surface modified TiO_2 and MgO nanoparticles.

MM onto AlN had only a minor effect on particle distribution in a 5 wt.% PP/AIN system, compared to untreated PP/AlN. Micron–size agglomerations could also be observed for MM in PP/MgO nanocomposites [8].

In contrast, functionalization with MA and EA containing amino groups appear to lead to enhanced dispersion and distribution of both TiO_2 and MgO, with agglomerate sizes reduced to 1–2 μm. This is in line with previous findings [1] [9], which reported that at filler contents >3 wt.%, PP/TiO_2/EA and PP/MgO/MA system were characterized by fewer micron–sized agglomerations. Nanoparticles treated with a polar SCA retain their hydrophilic properties and are less compatible with the nonpolar PP matrix. As a result, treated nanoparticles, which are strongly connected by polar–polar interactions, tend to agglomerate, resulting in a poor dispersion within the PP matrix, particularly in the case of MM, which has a more polar character.

C. Differential Scanning Calorimetry

DSC crystallization and melting data obtained from all tested nanocomposites is shown in Table II. It is evident that the *measured* peak melting temperature, T_m, of the nanocomposites is not significantly different from that of the unfilled PP. Similar results were also reported in [2] [9]. The degree of crystallinity, χ_c, was calculated using DSC melting curves based on (2) [1]:

$$\chi_c = \frac{\Delta H_m}{(1-w)H_0} \times 100\% \quad (2)$$

where ΔH_m is the melting enthalpy of PP nanocomposites, H_0=207 J/g [1] the melting enthalpy of 100% crystalline PP and w is the mass fraction of nanoparticle in the system. The resulting crystallinity values are presented in Table II. From this, it is evident that the DSC melting endotherm crystallinity values are invariant with composition, which is, again, in line with results presented elsewhere [2] [9]. Finally, consider the crystallization temperature, T_c, data in Table II, which reveals values of T_c in all the nanocomposites that are increased by, typically, 7–8 °C compared to unfilled PP. This is consistent with previous studies [1] [16] and significant in two respects. First, the peak temperature of the crystallization exotherm is determined by the rate of crystallization, which, in turn, is determined by the number of nuclei present in the system and the rate of subsequent crystal growth. Since, within this temperature range concerned here, the crystal growth rate increases with decreasing temperature, an elevation in T_c must therefore be indicative of increased nucleation. That is, the nanoparticle acts as a heterogeneous nucleating agent, which accelerates the crystallization process. Second, the changes in T_c are not reflected in the measured values of T_m, which is a consequence of reorganisation of the initial lamellar population during the course of the DSC scan, as is commonly observed for PP [17]. In conclusion, the DSC results reported here are in line with expectations and show that the primary consequence of adding MgO and TiO_2 nanoparticles to PP is to change the morphology through changes in the nucleation density. Neither the overall crystallinity nor the lamellar thickness is greatly affected.

D. Water Absorption

In Fig. 3, the change in mass of PP nanocomposites measured at room temperature after 21 days immersion in water is shown. All data were normalized with respect to the initial mass of each dried sample. Unsurprisingly, the variation in the mass of the unfilled PP was only around 0.02±0.01%; this insignificant change is due to the strongly hydrophobic nature of the nonpolar carbon chain structure of this polymer [18]. All nanocomposites absorbed more water than the unfilled PP and reached quasi–equilibrium after 3 days. The greater water absorption in PP nanocomposites can be attributed to the polar nature of these nanofiller surfaces, which interact strongly with water molecules [18] [19]. After 21 d of water immersion, the MgO– filled systems absorbed twice as much water as the TiO_2 analogues for untreated systems: 0.64±0.05% for MgO; 0.23±0.04% for TiO_2. The fact that the untreated MgO nanocomposite absorbs more water than the TiO_2 analogue implies either that the surfaces are more hydrophilic (e.g., more

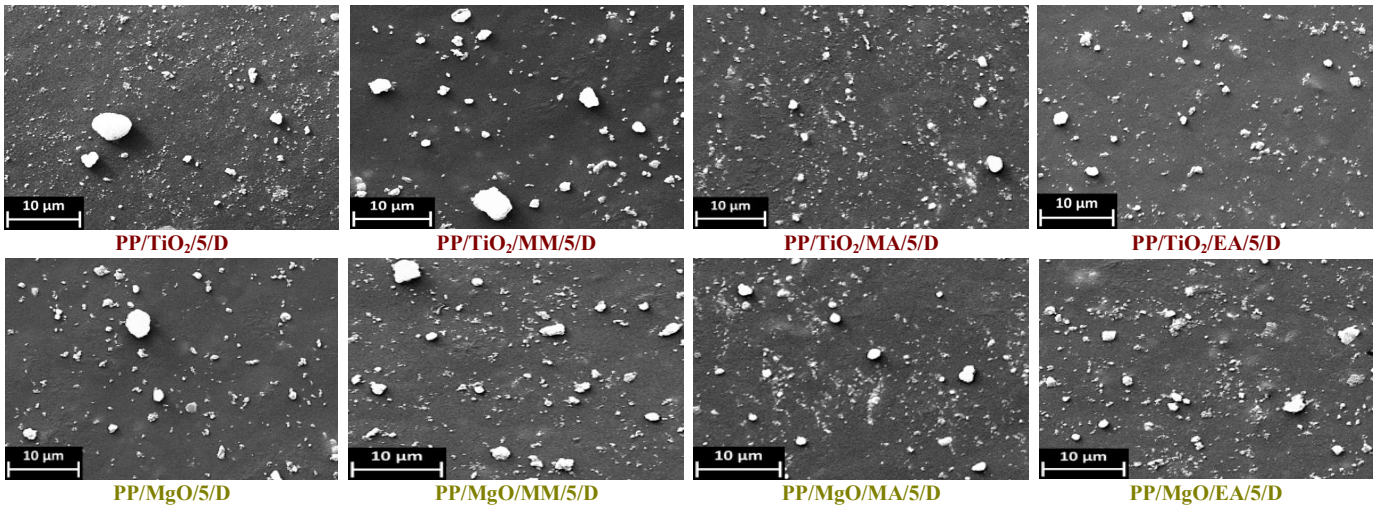

Fig. 2. SEM micrograph images of PP nanocomposite with 5 wt.% TiO_2 and MgO surface modified by different SCA.

TABLE II
DSC MELTING AND CRYSTALLIZATION RESULTS FOR PP NANOCOMPOSITS.

Sample Types	T_m (°C)	T_c (°C)	χ_c (%)
Neat PP	161.7	113	42.6
PP/TiO_2/5/D	161.5	118.7	43.2
PP/TiO_2/MM/5/D	162	118.3	43.8
PP/TiO_2/MA/5/D	161.6	118.5	43.8
PP/TiO_2/EA/5/D	160.3	117.7	44.6
PP/MgO/5/D	163.3	121.8	44.5
PP/MgO/MM/5/D	161. 7	119.7	44.9
PP/MgO/MA/5/D	161.8	119.8	44.7
PP/MgO/EA/5/D	161.2	119	44.9

–OH groups per nm^2) and/or that the surface area is great (with a constant –OH group density). This ties up rather well with the above discussion of the TGA data – increased grafting in MgO. From the analysis of the data presented in Fig. 1, the extent of reaction for the three SCA with TiO_2 is comparable. As such, the reduction in the amount of water absorbed by PP/TiO_2/EA/5/H compared with the two other functionalised PP/TiO_2–based systems suggests that this filler leads to reduced interactions with water. Indeed, this is consistent with the behavior exhibited by the MgO–filled systems, where the lowest water absorption was seen in PP/MgO/EA/5/H.

E. Dielectric Permittivity

Fig. 4 (a) and (b) show the frequency dependence of the real part of the relative permittivity, ε_r', obtained from dry PP nanocomposites containing 5 wt.% TiO_2 and MgO. An overview of such data has been discussed previously [20]; here, this analysis is expanded and used as the reference to discuss the impact of water absorption. The frequency dependence of ε_r' of samples immersed in water is presented in Fig. 4 (c) and (d).

Due to the low water uptake (<0.05%) of PP, the relative permittivity of wet and dry systems is virtually identical. Conversely, all nanocomposites exhibit higher relative permittivity values after water exposure, with the increase being greater for MgO nanocomposites than for TiO_2–based systems. For example, the permittivity increases at 1 Hz in systems containing MgO and MgO/EA is 0.4 and 0.24, respectively. At the same frequency, systems containing untreated TiO_2 and TiO_2/EA exhibit increases of around 0.32 and 0.23, respectively. The increase in ε_r' on water exposure is greater in systems containing untreated nanofiller than in systems containing the equivalent functionalized nanofiller. The increase in relative permittivity correlates well with the extent of water absorption.

The frequency dependence of the dielectric loss, tan δ, of the dry materials is presented in Fig. 5 (a) and 5 (b), while equivalent data obtained from the TiO_2– and MgO–filled systems after water immersion is shown in Fig 5 (c) and 5 (d),

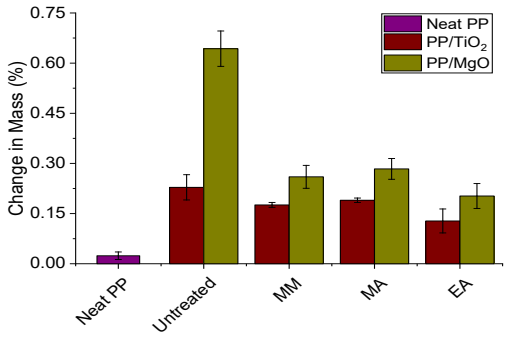

Fig. 3. Change in mass of water content of PP nanocomposites after 21 days compared to dry condition.

respectively. While tan δ was unaffected by water immersion for unfilled PP, distinct relaxation peaks can be observed in the nanocomposites [21]. The water content of the system containing untreated TiO_2 was around 0.41% lower than in the untreated MgO system. The system containing untreated TiO_2 exhibits a relaxation peak at ~1 Hz, whereas the relaxation peak in the system containing untreated MgO system is shifted to ~100 Hz. This is consistent with the water model proposed in [19], in which the frequency of the observed dielectric relaxation is related to the absorbed water content, other factors remaining constant. Initially water molecules are hydrogen bonded to nanoparticle surfaces, such that the associated relaxation peak manifests at a lower frequency [19] [22]. As the water content increases, the interfacial constraints diminish [19] and the relaxation peak is displaced to a higher frequency, clearly demonstrated here in the untreated MgO system.

From Fig. 3, it is evident that surface treatment has little impact on the quantity of water absorbed in TiO_2–filled systems. According to [19], the associated relaxation peak frequency should be largely invariant, which is not the case here. Comparing the systems containing untreated TiO_2, the relaxation peak frequency of the TiO_2/MA system is shifted to 2 kHz, a significantly higher frequency.

Due to the presence of polar moieties on the SCA chain, water molecules would interact not only with untreated surface groups, but also with other polar species [18]. In [22], where a nonpolar SCA was used, two overlapping relaxation peaks were observed, suggesting these were caused by two distinct sites for binding water. However, this is in contrast with the results of this study, where only a single relaxation peak for each system can be identified. The majority of water interacts with SCA polar moieties, rather than residual, unreacted surface groups are proposed. Cross–reaction of tri–SCA could form a thicker layer around the nanoparticle surfaces, which would inhibit interactions with free polar surface groups [16]. TGA results suggest that this would mainly occur in the MgO systems. Conversely, this is less likely in TiO_2 systems, where low SCA density values imply something close to a monolayer. The implication is that each SCA consumes only on –OH group, so the other two silanols on the SCA are free to react with one another.

Even with a change in water content of about ~0.1%, water molecules interacting with different polar moieties on SCA chain showed distinct bonding states. It appears that the water

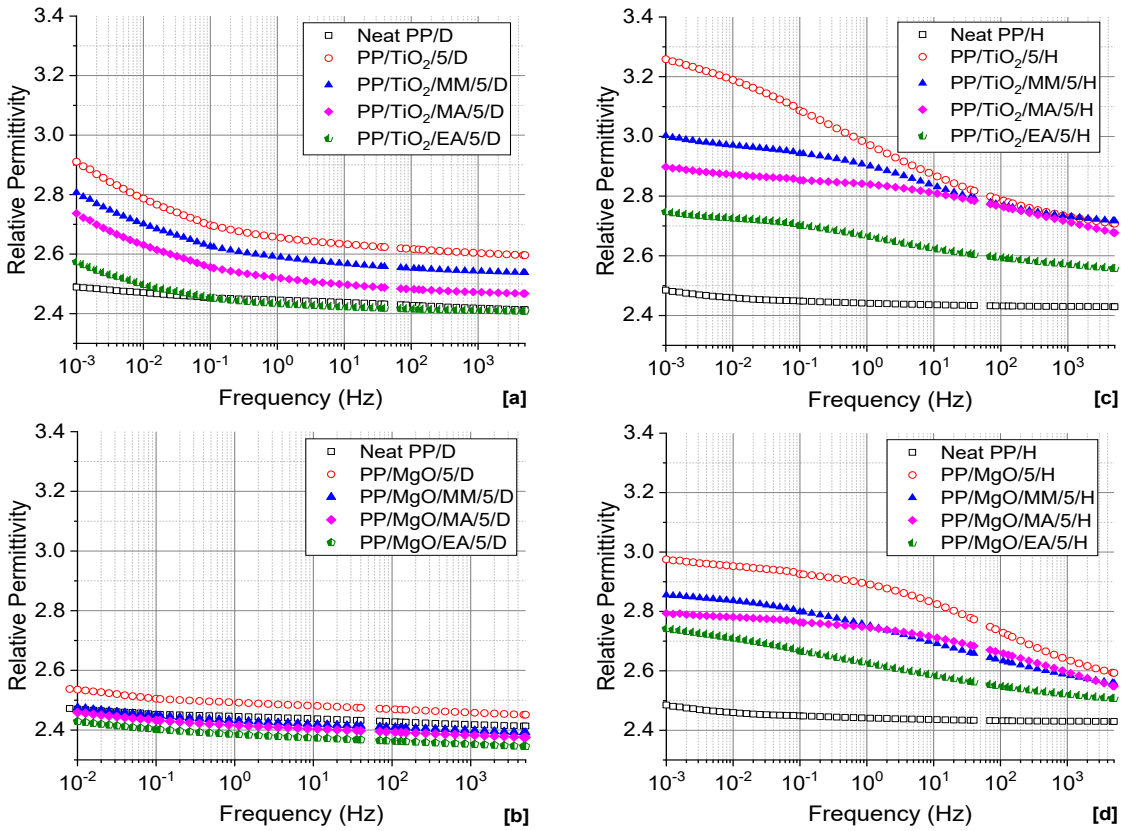

Fig. 4. Relative permittivity with different SCA in dry condition of (a) PP/TiO2/5/D: (b) PP/MgO/5/D and in humid condition of (c) PP/TiO2/5/H: (d) PP/MgO/5/H.

bonding states with polar species make dipolar relaxations easier, as evidenced by the higher relaxation peak frequencies in all treated TiO_2 systems.

In comparison to TiO_2–filled systems, MgO–filled systems showed a much larger difference in water content, ~0.45%, between untreated and treated samples. The water shell of an untreated particle should therefore be thicker than a successfully treated particle, at least according to the water shell model [19]. The relaxation peaks of treated systems should occur at a decreased frequency, as observed in MgO/MM and MgO/EA systems. The relaxation peak frequency in MgO/MA systems, on the other hand, was significantly higher than in untreated MgO.

The approximate water shell layer dimensions were calculated to put this behavior in context. For this calculation it was assumed that nanoparticles are spherical shape and are dispersed uniformly. Mass variations of samples were taken from humidity experiment results. The approximate radii of water shells around nanoparticles were thus calculated using the relationship between density (ρ), mass (M) and volume (V) of substances ($\rho = M/V$), with the findings summarised in Fig. 6. Untreated MgO have an about ~25% larger thicker layer than MgO/MA systems. This means that the different relaxation peak frequencies observed do not depend on the thickness of these water shells. Thus, it would be the different water bonding states with surface functional groups that is main determinant of the observed dielectric behavior.

Among SCA–treated samples, the effect of different relaxation peaks caused by different water bonding states can be clearly observed. Relaxation peak frequencies of MM, MA, and EA in both nanocomposites were at 10 Hz, 2 kHz, and 2 Hz respectively. Comparing the same surface functional groups, the MA system has the largest difference in the derived water shell thickness between TiO_2 and MgO samples of about 15%. Although the calculated water shell thickness of two systems differed, the relaxation peak frequencies remained the same. This underlines the relationship between dielectric permittivity of nanocomposites and the bonding states of water molecules.

In systems with untreated particles, the calculated water shell thicknesses differed by more than 30%, and different relaxation peak frequencies can be observed. This variation can be attributed to the different surface functional groups. As mentioned in the TGA section, apart from –OH functional groups, other oxygen–containing functional groups can exist on surface of nanoparticle used. When there are different ratios between –OH and other functional groups on TiO_2 and MgO surfaces, this results in different water bonding states, thus distinct relaxation peak frequencies. Different widths of relaxation peaks in systems with untreated particles support this hypothesis [22].

The magnitude of the loss peak differs significantly between dry and humid systems, especially in TiO_2 systems and less so for MgO. For example, in dry and humid conditions, the magnitude dielectric loss at low frequency (1 mHz) is 0.04 and

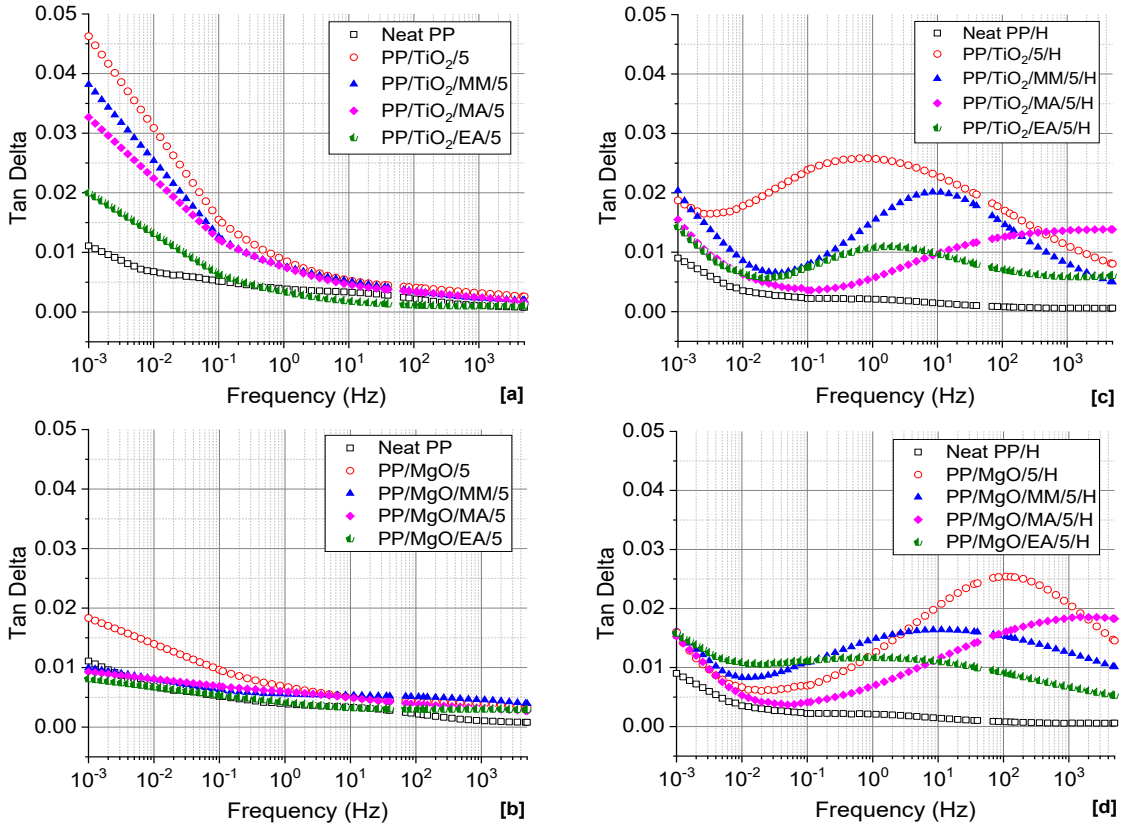

Fig. 5. Dielectric loss with different SCA in dry condition of (a) PP/TiO2/5/D: (b) PP/MgO/5/D and in humid condition of (c) PP/TiO2/5/H: (d) PP/MgO/5/H.

0.02, respectively. This high magnitude in dry TiO_2 systems is likely due to interfacial polarization of charge trapped at the interfaces [23] [24]. In humid conditions, the maximum magnitude of dielectric loss occurs during the relaxation peak at 1 Hz. This is most likely caused by the dipolar relaxation of the permanent dipole of water [25].

Two overlapping dielectric response mechanisms of dipolar and interfacial relaxations are present in humid conditions are assumed. This is confirmed by comparing dielectric permittivity in both conditions at frequencies of 20 µHz. At low frequencies, the magnitude of tan delta in both systems is comparable, as illustrated in Fig. 7. However, with MgO there were no significant changes in the dielectric loss magnitude. The interfacial polarization is simply not a dominant factor for the dielectric permittivity in dry MgO systems [20].

V. Conclusion

This work analyses the effects of different SCA on TiO_2 and MgO of same dimensions in PP under different humidity conditions. As observed in SEM images, nanoparticles treated with polar SCA have polar–polar interactions, resulting in a

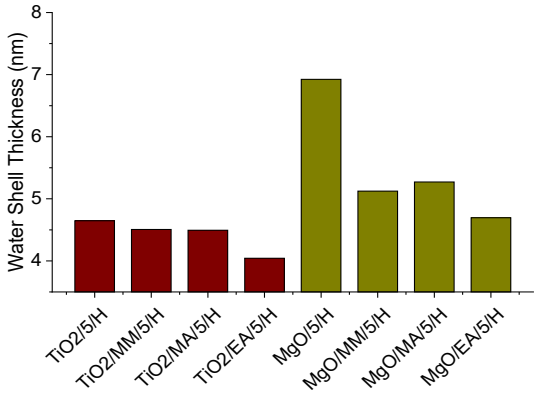

Fig. 6. Calculated water shell thickness of PP nanocomposites.

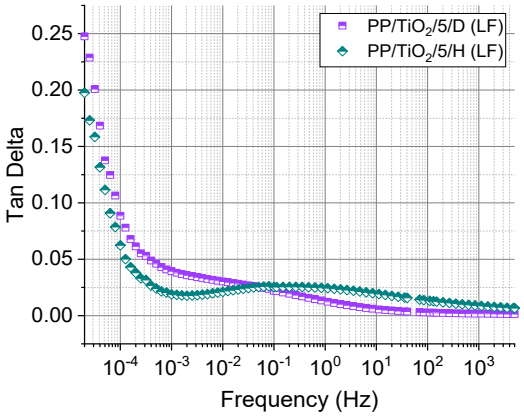

Fig. 7. Dielectric loss of untreated PP/TiO2/5 at 20 µH low frequency (LF).

poor nanofiller distribution, particularly with MM–SCA. Nanoparticles act as a heterogeneous nucleation agent, causing an increase of the crystallization temperature by 7–8 °C, compared to neat PP.

TiO_2 and MgO have significantly different surface structures for their SCA layers, with the estimated SCA graft density for MgO being 10 times higher than for TiO_2. More SCA functional groups, either self–condensation to form a thicker surface layer or more surface –OH groups to react with, imply that more polar molecules (such as water) can interact in MgO–filled systems. Although the amount of SCA is proportional to the water uptake, surface treatment drastically reduces the mass of water compared to the untreated samples.

After being immersed in water, nanocomposites have higher relative permittivity. The increases in relative permittivity in systems with SCA are less pronounced than in untreated samples, consistent with the presence of polarizable water molecules in the systems.

Different water bonding states due to distinct water layers are identified, where the relaxation peak frequency varies. Using different polar functional groups of SCA in this study demonstrates specific relaxation peaks related to different SCA types. The relaxation peaks of MM, MA, and EA are at 10 Hz, 2 kHz, and 2 Hz, respectively. However, the derived water shell thickness of different nanoparticle types with the same SCA groups can differ, while the relaxation peaks stay the same. It can be concluded that certain water bonding states from specific polarities on the SCA chain offer specific relaxation peaks, related to the molecular structure.

Relaxation mechanisms at low frequencies (<0.1 Hz) are dominated by interfacial polarization. When samples are exposed to moisture, two overlapping dielectric mechanisms of dipolar (permanent water dipole) and interfacial relaxation (charges trapped at the interface) occur. It can be clearly identified in which systems interfacial polarization is dominant, i.e., in TiO_2 nanocomposite.

In conclusion, that samples with ethoxy based amino functional groups result in the lowest dielectric permittivity, which would be attributed to the nitrogen–rich polar functional group. Here, only the dielectric permittivity has been taken into account. Future work will concentrate on the space charge dynamics with different SCA and moistures.

REFERENCES

[1] W. Cao, Z. Li, G. Sheng, and X. Jiang, “Insulating property of polypropylene nanocomposites filled with nano-MgO of different concentration,” *IEEE Trans. Dielectr. Electr. Insul.*, vol. 24, no. 3, pp. 1430–1437, 2017.

[2] G. Yu, Y. Cheng, and Z. Wu, “Effect of nano-MgO particles doping on breakdown characteristics of polypropylene,” *Coatings*, vol. 10, no. 4, p. 312, 2020.

[3] N. M. K. Abdel-Gawad, A. Z. El Dein, D. E. a. Mansour, H. M. Ahmed, M. M. F. Darwish, and M. Lehtonen, “PVC nanocomposites for cable insulation with enhanced dielectric properties, partial discharge resistance and mechanical performance,” *High Volt.*, vol. 5, no. 4, pp. 463–471, 2020.

[4] X. Wang, T. Andritsch, and G. Chen, “Effect of surface functionalization on the dielectric properties of polypropylene aluminium nitride nanocomposites,” in *IEEE International Conference on Dielectrics,* 2018.

[5] Y. Zhou, J. Hu, B. Dang, and J. He, “Effect of different nanoparticles on tuning electrical properties of polypropylene nanocomposites,” *IEEE Trans. Dielectr. Electr. Insul.*, vol. 24, no. 3, pp. 1380–1389, 2017.

[6] K. Y. Lau, A. S. Vaughan, G. Chen, I. L. Hosier, and A. F. Holt, “On the dielectric response of silica-based polyethylene nanocomposites,” *J. Phys. D Appl. Phys.*, vol. 46, p. 095303, 2013.

[7] Standard Test Methods for AC Loss Characteristics and Permittivity (Dielectric Constant) of Solid Electrical Insulation, ASTM D150-11 2018.

[8] Y. Zhou *et al.*, “Temperature dependent electrical properties of thermoplastic polypropylene nanocomposites for HVDC cable insulation,” *IEEE Trans. Dielectr. Electr. Insul.*, vol. 26, no. 5, pp. 1596–1604, 2019.

[9] Y. Zhou, J. Hu, B. Dang, and J. He, “Titanium oxide nanoparticle increases shallow traps to suppress space charge accumulation in polypropylene dielectrics,” *R. Soc. Chem.*, vol. 6, pp. 48720–48727, 2016.

[10] J. Gao, H. Liu, T. Lee, U. Schachtely, H. Kobayashi, and L. Li, “Effect of hydrophilic/hydrophobic nanostructured TiO2 on space charge and breakdown properties of polypropylene,” *Polymers (Basel).*, vol. 14, no. 14, p. 2762, 2022.

[11] G. Balakrishnan, R. Velavan, K. Mujasam Batoo, and E. H. Raslan, “Microstructure, optical and photocatalytic properties of MgO nanoparticles,” *Results Phys.*, vol. 16, p. 103013, 2020.

[12] P. Praveen, G. Viruthagiri, S. Mugundan, and N. Shanmugam, “Structural, optical and morphological analyses of pristine titanium di-oxide nanoparticles-synthesized via sol-gel route,” *Spectrochim. Acta-Part A Mol. Biomol. Spectrosc.*, vol. 117, pp. 622–629, 2014.

[13] X. Huang and P. Jiang, “Nanoparticle surface modification for dielctric polymer nanocomposite,” in *Tailoring of Nanocomposite Dielectrics from Fundamentals to Devices and Applications*, T. Tanaka and A. S. Vaughan, Eds. Pan Stanford Publishing Pte. Ltd, 2017, pp. 77–110.

[14] L. T. Zhuravlev, “The surface chemistry of amorphous silica. Zhuravlev Model,” *Colloids Surfaces A Physicochem. Eng. Asp.*, vol. 173, no. 1–3, pp. 1–38, 2000.

[15] X. Wang, T. Andritsch, G. Chen, and S. Virtanen, “The role of the filler surface chemistry on the dielectric and thermal properties of polypropylene aluminium nitride nanocomposites,” *IEEE Trans. Dielectr. Electr. Insul.*, vol. 26, no. 3, pp. 1009–1017, 2019.

[16] X. He *et al.*, “Silica surface-modification for tailoring the charge trapping properties of PP/POE based dielectric nanocomposites for HVDC cable application,” *IEEE Access*, vol. 8, pp. 87719–87734, 2020.

[17] Y. Zhao, A. S. Vaughan, S. J. Sutton, and S. G. Swingler, “On the crystallization, morphology and physical properties of a carified propylene/ethylene copolymer,” *Polymer (Guildf).*, vol. 42, no. 15, pp. 6587–6597, 2001.

[18] X. Wang, D. Qiang, I. Hosier, Y. Zhu, G. Chen, and T. Andritsch, “Effect of water on the breakdown and dielectric response of polypropylene/nano-aluminium nitride composites,” *J. Mater. Sci.*, vol. 55, pp. 8900–8916, 2020.

[19] C. Zou, J. C. Fothergill, and S. W. Rowe, “The effect of water absorption on the dielectric properties of epoxy nanocomposite,” *IEEE Trans. Dielectr. Electr. Insul.*, vol. 15, no. 1, pp. 106–117, 2008.

[20] P. Ketsamee, T. Andritsch, and A. Vaughan, “Effect of surface-modified TiO2 and MgO nanoparticles on dielectric permittivity and breakdown strength of PP nanocomposites,” in *IEEE Conference on Electrical Insulation and Dielectric Phenomena,* 2021.

[21] I. L. Hosier, M. Praeger, A. S. Vaughan, and S. G. Swingler, “The effects of water on the dielectric properties of aluminum-based nanocomposites,” *IEEE Trans. Nanotechnol.*, vol. 16, no. 2, pp. 169–179, 2017.

[22] N. Jäverberg *et al.*, “Dielectric properties of alumina-filled poly (ethylene-co-butyl acrylate) nanocomposites part II- wet studies,” *IEEE Trans. Dielectr. Electr. Insul.*, vol. 19, no. 2, pp. 391–399, 2012.

[23] A. Ridhore and J. P. Jog, “A dynamic mechanical and dielectric relaxation study of PP-g-MAH/clay nanocomposites,” *Open Macromol. J.*, vol. 6, no. 1, pp. 53–58, 2012.

[24] Prateek, R. Bhunia, S. Gupta, A. Garg, and R. K. Gupta, “In-situ fabrication of barium titanate@polyvinyl pyrrolidone in polyvinylidene fluoride polymer nanocomposites for dielectric capacitor applications,” *J. Polym. Sci.*, vol. 60, no. 6, pp. 961–967, 2022.

[25] I. L. Hosier, M. Praeger, A. F. Holt, A. S. Vaughan, and S. G. Swingler, “On the effect of functionalizer chain length and water content in polyethylene/silica nanocomposites: part I – dielectric properties and breakdown strength,” *IEEE Trans. Dielectr. Electr. Insul.*, vol. 24, no. 3, pp. 1698–1707, 2017.